The hot, warm and cold gas in Arp 227 - an evolving poor group

R. Rampazzo, P. Alexander, C. Carignan, M.S. Clemens, H. Cullen, O. Garrido, M. Marcelin, K. Sheth, G. Trinchieri

Mon. Not. R. Astron. Soc. **368,** 851–863 (2006) doi:10.1111/j.1365-2966.2006.10179.x

The hot, warm and cold gas in Arp 227 – an evolving poor group

R. Rampazzo,[1⋆] P. Alexander,[2] C. Carignan,[3] M. S. Clemens,[1] H. Cullen,[2] O. Garrido,[4] M. Marcelin,[5] K. Sheth[6] and G. Trinchieri[7]

[1]*Osservatorio Astronomico di Padova, Vicolo dell'Osservatorio 5, I-35122 Padova, Italy*
[2]*Astrophysics Group, Cavendish Laboratories, Cambridge CB3 OH3*
[3]*Département de physique, Université de Montréal, C. P. 6128, Succ. centre-ville, Montréal, QC, Canada H3C 3J7*
[4]*GEPI, Observatoire de Paris, 5 Place Janssen, 92195 Meudon Cedex, France*
[5]*Observatoire Astronomique de Marseille Provence, 2 Place Le Verrier, 13248 Marseille Cedex 04, France*
[6]*Division of Physics, Mathematics, and Astronomy, California Institute of Technology, 770 South Wilson Avenue, Pasadena, CA 91125, USA*
[7]*Osservatorio Astronomico di Brera, Via Brera 28, I-20121 Milano, Italy*

Accepted 2006 February 6. Received 2005 November 22; in original form 2005 May 6

ABSTRACT

Arp 227 represents a prototypical example of an interacting mixed pair of galaxies located in a low-density environment. We investigate the gas properties of the pair in the X-ray, Hα, H I and CO bands. We also detect two additional members of the group in H I which indicates that the pair constitutes the dominant members of a loose group.

The H I distribution shows a tail of gas that connects the spiral member, NGC 470, to the lenticular, NGC 474, showing that the two main members are currently undergoing interaction. The Hα emission reveals the presence of secondary components at the centre of NGC 470, superposed on the main component tracing the rotation of the galaxy. This latter maps a nearly unperturbed velocity field. The dominant, nearly unperturbed trend of the kinematics is confirmed by CO observations, although restricted to the centre of the galaxy. The X-ray luminosity of NGC 470 is comparable with that of a 'normal' spiral galaxy. NGC 474 on the other hand is very gas-poor and has not been detected in Hα. Its X-ray luminosity is consistent with the low end of the expected emission from discrete sources.

Arp 227 as a loose group shows several signatures of galaxy–galaxy interaction. Our observations suggest the presence of signatures of interaction in the overall kinematics of the spiral companion. The ongoing interaction is clearly visible only in the outer H I halo of NGC 470. While the large shell system of NGC 474 could be associated with an accretion event, the secondary components in the Hα profile in the centre of NGC 470 could be due to the interaction with the companion. The low X-ray luminosity of NGC 470 seems to be a characteristic of dynamically young systems. All the above evidence suggest that Arp 227 is an evolving group in the early phase of its evolution and that its drivers are the accretion of faint galaxies and the ongoing large-scale interaction between NGC 470 and 474.

Key words: galaxies: evolution – galaxies: interactions – galaxies: individual: NGC 470 – galaxies: individual: NGC 474 – galaxies: kinematics and dynamics.

1 INTRODUCTION

The latest results from large spectroscopic surveys (Lewis et al. 2002) conclude that environmental influences on galaxy properties are effective well outside cluster cores, at local galaxy densities more typical of the group environment (Bower & Balog 2004). Given that such environments today contain a substantial fraction of the mass in the Universe, this would imply that the local environment strongly affects the evolution of most galaxies. Whether it is the cluster or the group environment that most strongly affects galaxy evolution is still an open and debatable question because our knowledge of galaxy evolution within low-density environments is still very poor.

Poor galaxy aggregates deserve special attention because they are the simplest systems where one can investigate the effects of interaction on their evolution. Pairs of galaxies represent about 10 per cent of the local non-cluster population and are particularly interesting because of the potentially accelerated effects on the secular evolution compared with unpaired galaxies in low-density environments. Observational signatures of secular evolution are indeed

⋆E-mail: rampazzo@pd.astro.it

present in binary galaxies. Optical and far-infrared (FIR) studies of pairs (Sulentic 1989; Xu & Sulentic 1991; Hernandez–Toledo & Puerari 1999; Hernandez–Toledo, Dultzin-Hacyan & Sulentic 2001; Nikolic, Cullen & Alexander 2004) show unambiguous evidence for interaction-induced star formation in the spiral components of the pairs at odds with, e.g. compact groups which show a low fraction of galaxies with signatures of a past interaction and no evidence of enhanced FIR emission (Zepf & Whitmore 1991; Zepf 1993; Verdes-Montenegro et al. 1998).

Among physical pairs, mixed binaries, i.e. pairs composed of an early- and a late-type galaxy, are interesting for two main reasons.

(i) They are clearly a site of galaxy evolution: recent Infrared Space Observatory (ISO) and Hα observations of 17 mixed pairs indicate that some of the early-type components are cross-fuelled by their spiral companions (Domingue et al. 2003). Support for this comes from the evidence of a significant population of early-type components with active galactic nucleus/low-ionization nuclear emission-line region (AGN/LINER)/H II galaxy spectroscopic properties in mixed pairs compared to the results from a similar survey of spiral–spiral pairs (Xu et al. 2000). Longhetti et al. (1999, 2000) analysed line-strength indices of 30 elliptical galaxies (E) members of interacting pairs suggesting that at least a fraction of them should have experienced a secondary episode of star formation which could explain their apparent *youth* in the Hβ versus MgFe plane.

(ii) In a hierarchical evolution scenario, pairs could represent the debris of older associations evolving towards more compact but poorer associations (Diaferio, Geller & Ramella 1994; Governato et al. 1996). The elliptical in mixed pairs could be the result of a merger (see e.g. Rampazzo & Sulentic 1992) and the pair itself a way station towards isolated elliptical galaxies as suggested by simulations (see e.g. Barnes 1996; Struck 1999) and recently by X-ray observations (see e.g. Mulchaey 2000).

With the present work, we present a multiphase study of the gas in Arp 227, a prototypical example of a galaxy–galaxy encounter in a low-density environment with clear signatures of ongoing interaction that we analyse in the context of the above scenario. The pair is composed of a barred spiral, NGC 470, and a lenticular, NGC 474, showing a spectacular shell system (Malin & Carter 1983). Since shells are generally considered to be generated through merging events between galaxies of different masses [mass ratios typically 1/10–1/100; Dupraz & Combes (1986); Henquist & Quinn (1987a,b)], the pair offers a snapshot of the secular galaxy evolution in the so-called field and probably also offers valuable insight about poor group formation and evolution.

This paper is organized as follows. Results from relevant studies in the literature about Arp 227 are summarized in Section 2. In Section 3, we present results coming from our observations of the hot, warm (Hα) and cold atomic (H I) and molecular (CO) gas components detected in the pair members. In Section 4, results are discussed in the light of available studies on group/pair evolution. We adopt $H_0 = 75$ km s^{-1} Mpc^{-1} and J2000 coordinates throughout.

2 ARP 227 IN THE LITERATURE

Arp 227 is an interacting pair composed of NGC 474, a lenticular and NGC 470, a spiral galaxy, separated by ≈5.4 arcmin. Table 1 summarizes the basic photometric and kinematical data of each member of the pair.

Table 1. Overview of Arp 227.

	NGC 470	NGC 474	References
Morphol. type	SA(rs)b	RSA(r)0	1
Hel. Sys. Vel. (km s^{-1})	2374±3	2373±7	1
Apparent magnitude and colours			
B_T	12.53±0.13	12.37±0.13	1
$\langle(B-V)_T\rangle$	0.75±0.11	0.88±0.02	4
$(U-B)_T$	0.10±0.05	0.38±0.03	1
$(J-H)_{2MASS}$	0.67	0.69	
$(H-K)_{2MASS}$	0.31	0.25	
Galaxy structure			
Effective surf. bright. μ_e(B)	22.04	22.96	4
Effective aperture A_e(B) (arcsec)	57.2	64.6	4
Average ellipticity $\langle\varepsilon\rangle$	0.31±0.09	0.16±0.12	4
$\langle\Delta$ PA$\rangle$ (deg)	≈ 63	≈33	4
Fine structure parameter (Σ)		5.26	5
Kinematical parameters			
Vel. disp. σ_0 [km s^{-1}] stars	56±31	163±5	2 and 3
Vel. disp. σ_0 [km s^{-1}] gas	84±8		2
Max. rotation V_{max} [km s^{-1}]		30±6	3
Arp 227 as a pair			
Projected separation (arcmin) (kpc)	5.4 (49.6)		
ΔV (km s^{-1})	≈0		
Adopted distance (Mpc)	31.6		

References: (1) de Vaucouleurs et al. (1991); (2) Vega Beltran et al. (2001); (3) Simien & Prugniel (2000) and (4) Pierfederici & Rampazzo (2004). The large position angle variation in NGC 470 is due to the bar presence. The position angle and ellipticity variation with radius have been fixed in the NGC 474 outskirts due to the presence of shells. The adopted distance is obtained using $H_0 = 75$ km s^{-1} Mpc^{-1}. The fine structure parameter, Σ, is obtained from Schweitzer et al. (1990).

Fig. 1 shows the shell system around NGC 474 only partially visible in Digitized Sky Survey (DSS) images. The complex system of shells in NGC 474 extends for several arcmin. Some of the features are more reminiscent of tail/loop structures than shells. Among these features, the 'comma-like' structure at ≈210 arcsec south-west (SW) of the galaxy centre is really spectacular. It seems to be a part of a long tail that extends east–west and passes the sightline towards the galaxy centre, up to the southern edge of the easternmost shell at 202 arcsec from the centre of the galaxy. A wide, faint ripple at the south-east edge of the galaxy is also visible and extends well outside the CCD frame shown in Fig. 1.

The two galaxies have a virtually null velocity difference. NGC 470 is undergoing an intense burst of star formation and has a weak bar (Friedli et al. 1986), a feature often generated during an encounter in a disc galaxy [see e.g. *N*-body simulations by Noguchi (1987)]. Schiminovich et al. (1997) report an H I tidal bridge connecting the two galaxies. Both evidences suggest an ongoing interaction. At the same time, the kinematics of NGC 470, obtained from long-slit spectroscopy, appear unperturbed, and the analysis done by Vega Beltran et al. (2001) shows that the ionized gas corotates with stars within the inner 60 arcsec.

The surface photometry (see e.g. Schombert & Wallin 1987; Turnbull, Bridges & Carter 1999; Pierfederici & Rampazzo 2004) indicates that NGC 474 is an S0 galaxy with a smooth and undistorted inner luminosity profile. The colour of the inner shells is consistent with the colour of the parent galaxy (see Table 1). For the outer shells, there is a discordant measure of their colour: they are significantly bluer according to Turnbull et al. (1999) and Pierfederici & Rampazzo (2004), but not according to Schombert & Wallin (1987).

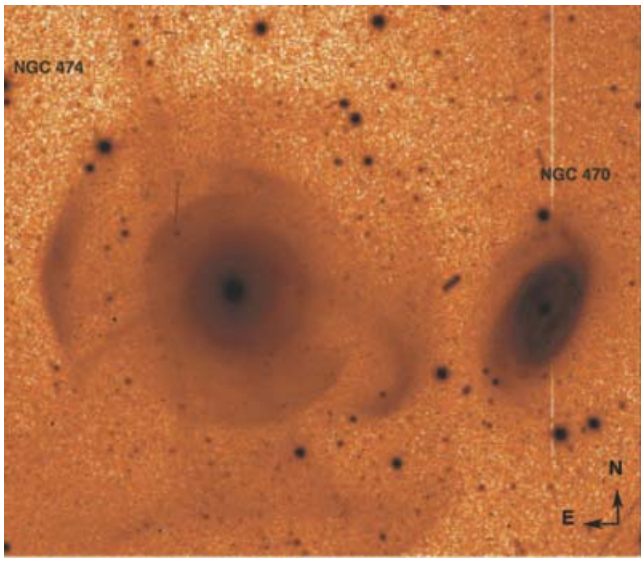

Figure 1. *B*-band image of Arp 227 obtained at the 1.5-m telescope at OHP (France). The field of view is 11 × 9.5 arcmin^2 [adapted from Pierfederici & Rampazzo (2004)].

The origin of the shells in NGC 474 has been debated by the above authors. On the grounds of their colours and surface brightness distribution with radius, shells could be produced by the weak interaction with NGC 470 or by the ingestion of a small satellite. The outer shells could also be the result of a mass transfer from NGC 470 (Turnbull et al. 1999). In this context, two contradictory pieces of evidence come from the observations. *H*-band *Hubble Space Telescope* (*HST*)/Near Infrared Camera and Multi-Object Spectrometer (NICMOS) surface photometry of the inner part ($r < 10$ arcsec) of NGC 474 confirms that the inner regions are undisturbed, showing no evidence for significant structures or dust (Ravindranath et al. 2001). In contrast, Hau, Balcells & Carter (1996) show that the core kinematics ($R < 5$ arcsec) in NGC 474 are peculiar: the core rotates around an axis intermediate between the photometric major and minor axes, suggesting that the galaxy is not a face-on S0 but rather a triaxial object. Hau & Thomson (1994) have proposed a model in which the mechanism for the formation of kinematically decoupled cores is the flyby interaction with another galaxy. The interaction with NGC 470 might then be responsible both for the inner shells and for the kinematically decoupled core of NGC 474. Another possibility is that the acquisition of a small object might have modified the inner kinematics (Kormendy 1984; Balcells & Quinn 1990). This second hypothesis is supported both by the measure of the trend of the shell surface brightness (Pierfederici & Rampazzo 2004), which is found to be basically flat [at odds with weak interaction models (Thomson 1991)] and by the increase of the shell in contrast with distance from the centre, a characteristic that the models of Hernquist & Spergel (1992) explain in the context of a merging event.

3 OBSERVATIONS AND RESULTS

3.1 The ionized gas

Observations of both NGC 470 and 474 were carried out in 2003 October with the GHASP instrument.[1] The instrument was attached to the f/15 Cassegrain focus of the 1.93-m telescope at the Observatoire de Haute Provence (OHP), France, and brought, through a focal reducer, to an aperture ratio of f/3.9. The detector was an Image Photon Counting System (IPCS) camera, based on the GaAs tube technology (Gach et al. 2002). This detector has a high quantum efficiency, zero readout noise and a very short readout time, which allow short exposures per channel avoiding transparency changes. Several cycles can then be done, and sky changes are averaged.

Table 2. GHASP observational parameters.

Observations	
Date (2003 Oct)	
Interference filter	
Central wavelength (Å)	6590
FWHM (Å)	15
Transmission (max)	0.67
Calibration	
Neon comp. light (λ Å)	6598.95
Perot–Fabry	
Interference order (at 6562.78 Å)	798
Free spectral range (at Hα (km s^{-1}))	376
Finesse at Hα	12
Spec. resolution at Hα	9400 (for S/N = 3)
Sampling	
No of scanning steps	24
Sampling step (Å) (equiv. 15 km s^{-1})	0.26
Pixel size	0.68 arcsec
Detector	GaAs tube
Field of view	5.8×5.8 arcmin^2
Exposures times	
Total exp. (h)	2
Total exp. time/chan. (s)	150
Eleme. exp./chan. (s)	10

Table 2 summarizes the observations. The reduction of the data cubes was performed using the ADHOCW software (Boulesteix 1999). The data reduction procedure has been extensively described in Amram et al. (1996).

Wavelength calibration was obtained by scanning the narrow Ne 6599-Å line under the same conditions as the observations. Velocities measured relative to the systemic velocity are very accurate, with an error of a fraction of a channel width (<5 km s^{-1}) over the whole field.

The signal measured along the scanning sequence was separated into two parts: (i) an almost constant level produced by the continuum light in a 15-Å passband around Hα (continuum map) and (ii) a varying part produced by the Hα line (Hα integrated flux map). The continuum level was taken to be the mean of the three faintest channels to avoid channel noise effects. The Hα integrated flux map was obtained by integrating the monochromatic profile in each pixel. The velocity sampling was 12 km s^{-1}. Strong OH night sky lines passing through the filter were subtracted by determining the level of emission away from the galaxies (Laval et al. 1987). The data cube of NGC 474 was analysed with the same procedure, but no Hα signal was detected after 2 h of observations. In the case of NGC 470, we derived the Hα distribution and the velocity map which are shown in Fig. 2.

[1]The instrument GHASP (Gassendi Hα survey of Spirals) belongs to the Laboratoire d'Astrophysique de Marseille.

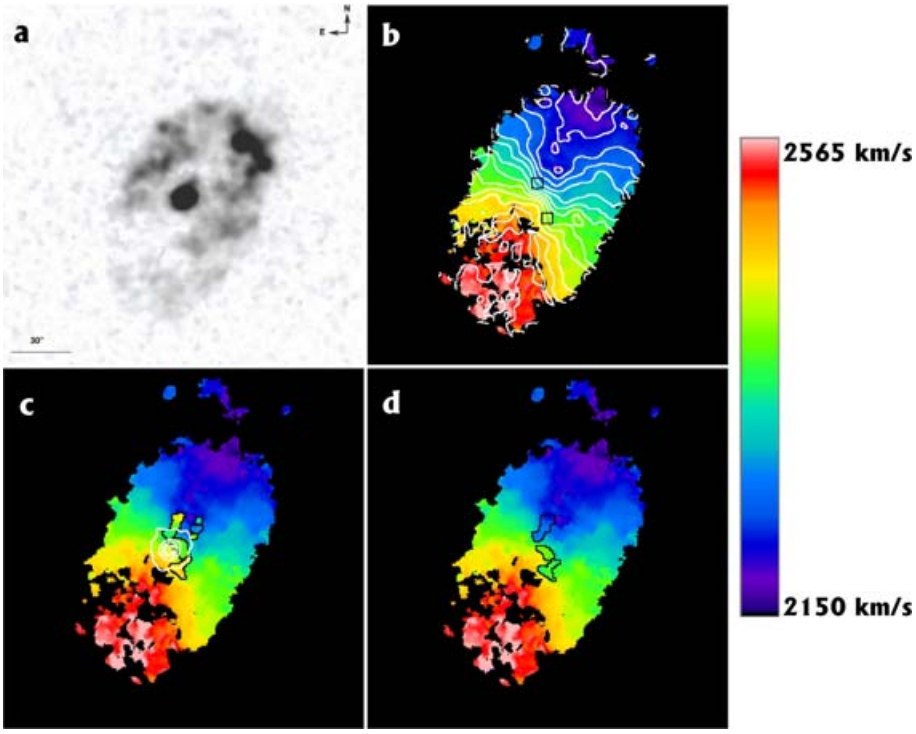

Figure 2. Hα distribution (panel a) and velocity field of NGC 470 (panel b). The step of the isovelocity contours is 25 km s^{-1}. The range of the velocity shown in the figure is given to the right. The central isophotes of continuum, indicating the galaxy centre, and the high- and the low-velocity parts of the second component in the Hα line profile are shown in panels c and d, respectively (these high- and low-velocity secondary components are localized in discrete areas in the centre, superposed here on the general velocity field). The total field of view of each panel is 2.9 $\times$2.9 arcmin^2. The two small squares, north and south of the nucleus in panel b, cover the selected areas of double profiles shown in Fig. 3.

The ionized gas distribution shows a ring-like structure at $\approx$30 arcsec from the centre. The bar structure formed by the stars at position angle (PA) $\approx$19° is not visible in the ionized gas distribution (moment zero Hα map; Fig. 2a), but is possibly responsible for the straight and parallel velocity contour seen towards the centre of the velocity map (moment 1 Hα map; Fig. 2b). The structure of the Hα map probably indicates that the bar is not sufficiently strong to induce star formation along its leading edge (Sheth et al. 2002). The velocity map of NGC 470 shows an overall regular velocity field that can be followed out to $\approx$100 arcsec.

At the same time, secondary components can be seen in the Hα line, superposed on the main component which traces the rotation of the galaxy. Each component has been mapped carefully by continuity from one pixel to the next, thus producing the different maps of Figs 2(c) and (d) for the high- and low-velocity component, respectively. Fig. 3 (panels a and b) shows two selected zones, within the above areas, where the two secondary components in the Hα profile are clearly visible. The area covered by the secondary velocity component extends along a kind of large S-shaped filament, 30-arcsec long and 5-arcsec wide, winding around the galaxy's stellar nucleus but slightly off-centred with respect to it. The double component in the Hα line profile does not seem clearly connected with the stellar bar which is, in addition, not aligned with the filament. There is also a small area, $\approx$15 arcsec north-west of the nucleus, where the high-velocity component can be seen superposed on the main component of the galaxy. The largest velocity differences between the two components are found to the north of the nucleus at 15 arcsec (200 km s^{-1}) and to the south-west at $\approx$10 arcsec (100 km s^{-1}).

3.2 The atomic gas

H I observations of Arp 227 were obtained from the Very Large Array (VLA) archive. Arp 227 was observed in D-array configuration on 1995 May 25, June 1 and 3 by D. Schiminovich. A correlator mode was used with 31 channels and a velocity width per channel of 41.9 km s^{-1} (195 kHz). The pointing centre was RA01^{h}20^{m}07^s.059, Dec. +03°25′01″.368(J2000), and the bandwidth was centred on a heliocentric radial velocity of 2446 km s^{-1}. The total integration time on-source was approximately 12 h. 0134+329 was used as a flux density calibrator with an assumed flux density of 15.98 Jy. On-source scans were interleaved with those of the phase calibrator, 0106+013.

Data reduction followed standard procedure using the National Radio Astronomy Observatory (NRAO) Astronomical Image Processing System (AIPS). The *uv* data sets were flagged as required and combined. Channel maps were made at an angular resolution of 69.93$\times$61.92 arcsec^2, using a *uv* taper of 2.5 kλ to bring out the extended structure. Subtraction of the average of the line-free channels was used to remove the continuum emission. For this purpose, the line-free channels were taken to be Channels 2–8 and 24–30, with the end channels being omitted due to their high noise levels. Channel maps 9–22 were summed in MOMNT using a combination of 'cut-off' and 'window' methods to optimize the detection of the H I. A flux cut-off of 0.28 mJy was used with smoothing functions of five cells in both velocity and spatial coordinates.

The VLA D-Array H I map in Fig. 4 reveals a tidal tail structure to both the east and west of NGC 470. The tail to the east is more extended, with low-level emission being detected east of NGC 474. The atomic gas distribution is strongly condensed on to

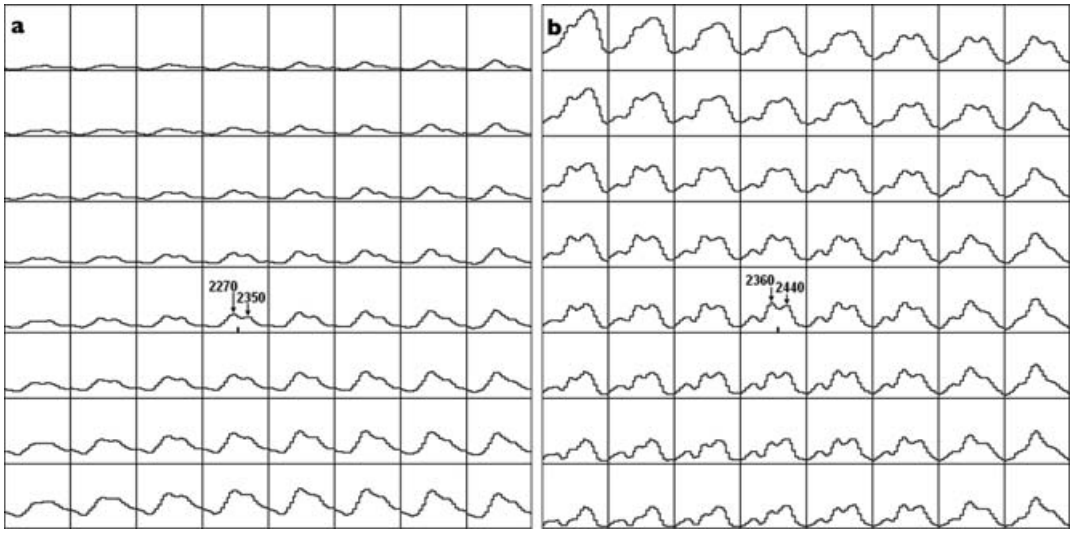

Figure 3. The Hα profiles are shown here for individual pixels in two selected areas where two components are clearly seen. The first area (panel a) is centred at about 1-arcsec west and 6.5-arcsec north with respect to the nucleus. The second area (panel b) is centred at about 5-arcsec west and 10-arcsec south with respect to the nucleus. Each area covers 5.44 × 5.44 arcsec^2 on the sky (8 × 8 pixels). Their location is shown in Fig. 2b. The velocity range of the profiles is between 2088 and 2466 km s^{-1} in the first (where the two components are found around 2270 and 2350 km s^{-1}) and between 2182 and 2560 km s^{-1} in the second one (where the two components are found around 2360 and 2440 km s^{-1}) as indicated in the central pixel of each area. The velocity of the main component is also indicated by the tick mark under the profile in the same panel. Note that the profiles exhibit an increasing continuum emission in the lower part of the first area (panel a), towards the nucleus of the galaxy.

the centre of the optical emission. Using the naturally weighted data ($\theta_{\rm FWHM} = 48.48 \times 46.65$ arcsec^2), the peak H I flux is 3.0 Jy beam^{-1} km s^{-1} corresponding to a column density of 1.5×10^{21} cm^{-2}. The flux level in the tidal tail is at a significantly lower level, peaking at around 0.2 Jy beam^{-1} km s^{-1} (1×10^{20} cm^{-2}). The integrated H I D-Array flux over the velocity range 2194–2655 km s^{-1} is 15.8 ± 0.3 Jy km s^{-1}. The H I flux of Arp 227 corresponds to an H I mass of 4.3×10^9 M$_\odot$. About 10 per cent of the H I emission detected is associated with tidal features, the larger part of the atomic gas remaining bound to NGC 470. The small fraction of total H I observed in the tidally stripped gas suggests that this system is in the early stages of interaction.

The western tidal tail has a velocity range of 2490–2520 km s^{-1}, whilst the eastern tail displays a broader range of 2340–2486 km s^{-1}. The velocities observed within the tidal features lie within the range defined by the atomic gas rotating with NGC 470. The average linewidths observed within the tidal features are 30 km s^{-1}. The linewidths grow to a maximum value of 118 km s^{-1} at the base of the western tidal extension, where the velocity of the atomic gas rotating with NGC 470 and that associated with the tidal tail differs markedly. The small H I cloud north of NGC 470 is also certainly connected with the Arp 227 system given its radial velocity (see Fig. 4, lower panel). This is presumably debris from the ongoing tidal encounter.

The general pattern of the central velocity field of NGC 470 is that of circular rotation, with the southern side of the galaxy redshifted and the northern side blueshifted (Fig. 4, bottom panel). The velocity field of the atomic gas, coincident with the optical emission, is traced by roughly evenly spaced isovelocity contours, parallel to the optical minor axis of the galaxy, characteristic of a rotating H I disc. The low-resolution data show a uniform velocity gradient across the central H I distribution, but this is a signature of the low spatial resolution of the data.

Examining the H I emission located beyond the optical galaxy, we observe a change in the orientation of the isovelocity contours. Near the centre, the contours are oriented nearly parallel to the galaxy minor axis, whereas at larger radii they are almost parallel to the major axis. The bottom panel in Fig. 4 shows the clear S-type distortion in the velocity field of NGC 470. This distortion is consistent with a warped H I disc and may be a result of the tidal disruption of the extended atomic gas.

In addition to Arp 227, two other galaxies have been detected in H I within the primary beam of the VLA. These are MCG 00-04-083 and [HDL97] 385–007. Their systemic velocities are 2262 and 2173 km s^{-1}, respectively, i.e. with a velocity separation $\Delta V <$ 200 km s^{-1} with respect to the Arp 227 pair and maximum projected separation of ≈20 arcmin (≈180 kpc). Classical group detection surveys (see e.g. Ramella et al. 1994) search for companions in a neighbourhood with a characteristic radius of 1.5 h^{-1} Mpc and within a velocity range 1500 km s^{-1} from the median of the group systemic velocity. The detected galaxies are well within this range, and it is very likely therefore that Arp 227 is part of a loose group.

3.3 The cold molecular gas

Berkeley Illinois Maryland Association (BIMA) ^{12}CO($J = 1 - 0$) observations were made of NGC 470 on 2003 October 5 and 19 with 10 telescopes in C configuration. NGC 470 was observed with a single pointing centred on RA 01$^{\rm h}$19$^{\rm m}$44$^{\rm s}$.50, Dec. + 03°24′42″.00 (J2000). Each observing run was approximately of 6 h, with a total time of 8 h 59 min on source. The phase calibrator was the quasar 0108+015, and the bandpass calibrator was 3C84. The total bandwidth was 368 MHz (960 km s^{-1}) centred on the velocity 2373 km s^{-1}, with a resolution of 1.56 MHz (4.06 km s^{-1}). The single-sideband system temperatures averaged ∼500 K on October 5 and ∼400 K on October 19.

Data reduction was carried out using standard reduction algorithms from the MIRIAD package (Sault, Teuben & Wright 1995). The flux of the phase calibrator was assumed to be 2.2 Jy based on the ratio of the observed fluxes of 3C84 and 0108+015 during the

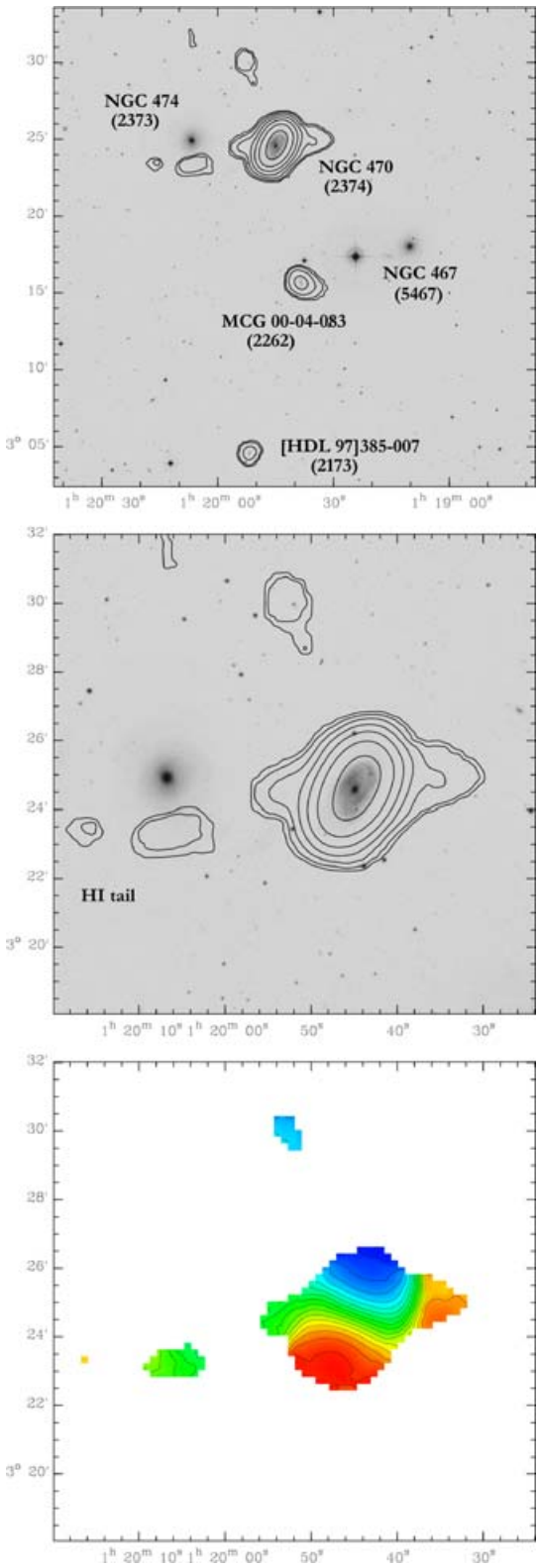

Figure 4. Top panel: H I emission in the Arp 227 system. The main galaxies in the area and their systemic velocities are indicated. NGC 467 does not belong to the Arp 227 system. Contour levels are at (0.05, 0.1, 0.2, 0.4, 0.8, 1.6, 3.2) Jy beam^{-1} km s^{-1} ($\theta_{\rm FWHM} = 69.33 \times 61.92$ arcsec^2). Middle panel: enlargement of the top panel to show in more detail the H I tail induced by the interaction. Bottom panel: intensity-weighted mean velocity field of the Arp 227. Contour levels run from 2240 to 2540 with a separation of 20 km s^{-1}, and the colour scale goes from 2230 (blue) to 2550 km s^{-1} (red).

observations and calibration observations of 3C84 made at BIMA shortly before and after our observations. Data with anomalous visibilities resulting from antenna shadowing at low elevation and noisy data at the edge of the correlator windows were flagged. In addition, all data from antenna 3, which appeared noisy throughout both the sets of observations, were flagged and discarded.

The *uv* data sets were exported from MIRIAD to AIPS where channel maps were made at a velocity resolution of 30 km s^{-1}. A *uv* taper of 14 kλ was applied in one orthogonal direction in the uv plane to correct for the distorted oval shape of the beam, producing maps of angular resolution $\theta_{\rm FWHM} = 10.43 \times 9.19$ arcsec^2. Emission was detected in Channels 12–25 corresponding to a velocity range of 2220–2480 km s^{-1}. Channels 12–25 were summed in the AIPS task MOMNT using a combination of the 'cut-off' and 'window' methods; a flux cut-off of 40 mJy was used with smoothing functions of four cells in both the velocity and spatial coordinates.

The ^{12}CO($J = 1 - 0$) emission in NGC 470 is centrally condensed. The full width half maximum of the BIMA primary beam at 115 GHz is 100 arcsec probing the full optical extent of the late-type galaxy NGC 470; none the less, emission is only detected in the very central region of this system. The emission appears essentially unresolved, revealing a slight distortion towards the north-west of the galaxy (Fig. 5, top panel).

The total linewidth of the ^{12}CO($J = 1 - 0$) emission is 280 km s^{-1}. Integrating over this line from Channel 12 (2480 km s^{-1}) to 25 (2220 km s^{-1}), we obtain a CO flux of 127 $\pm$ 25 Jy km s^{-1}. Assuming a CO-to-H_2 conversion factor, $X \equiv N(H_2)/I_{\rm CO} = 2.8 \times 10^{20}$ cm^{-2} km s^{-1}, we obtain a total mass of H_2 for NGC 470 of 1.6×10^9 M$_\odot$. The velocity field of the molecular gas emission in NGC 470 indicates circular rotation (Fig. 5, bottom panel). Like the velocity field of the atomic gas, that of the molecular gas is traced by roughly evenly spaced isovelocity contours parallel to the minor axis of the galaxy, but the rotation gradient is much higher than that seen in the H I data.

3.4 The hot gas

We obtained *XMM–Newton* observations of NGC 474 with European Photon Imaging Camera (EPIC) in the medium filter on 2004 January 24. Standard reduction was applied to the data mainly with SAS version 5 (http://xmm.vilspa.esa.es), but we also made use of both CIAO and DS9/FUNTOOLS (http://cxc.harvard.edu/ciao/).

The *XMM–Newton* data were heavily affected by periods of high background. Cleaning of the original data resulted in net exposures of ∼4.3 ks for the EPIC–PN instrument and of ∼11.4 ks for the EPIC–MOS (Metal Oxide Semiconductor), a considerable reduction from the original ∼19-ks exposures.

To improve the statistics without having to take into account the different patterns in the CCD gaps in the two instruments, we have summed all EPIC–MOS data and kept the EPIC–PN data separate.

The isointensity contours derived from the adaptively smoothed EPIC–MOS data are plotted on to the optical image from the DSS-II in Fig. 6. Only the photons in the 0.3–3.0 keV band were used. A very faint source is detected at the position of NGC 474, whereas a more complex emission is associated with NGC 470. The component to the west is probably a background source (see Appendix A). A few other sources are also detected and coincide with faint optical counterparts (mostly stellar in appearance).

The poor statistics that result from this data set do not allow us to investigate in detail the X-ray characteristics of the two galaxies. Table 3 summarizes the relevant X-ray measures for both galaxies.

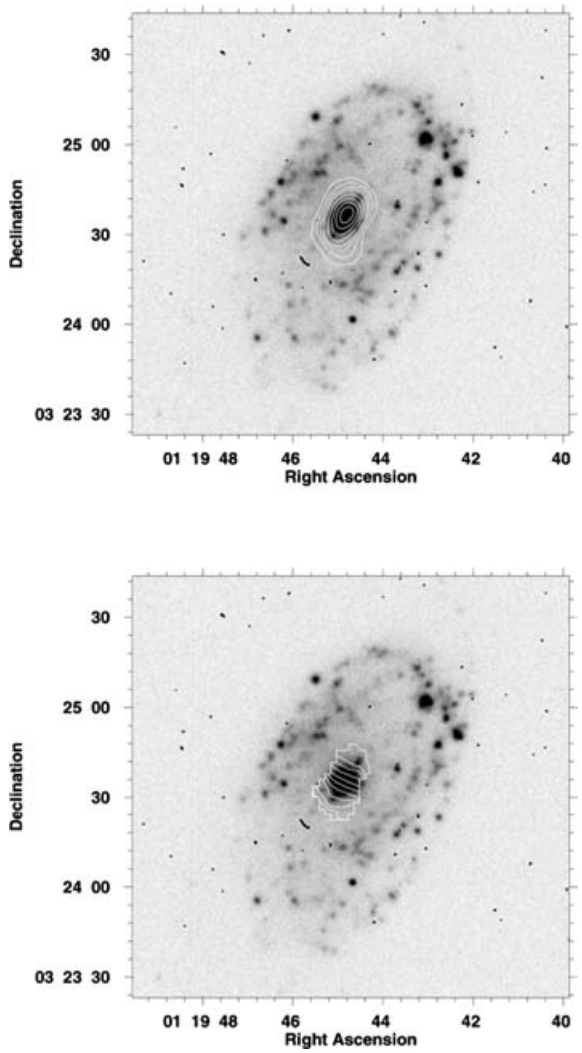

Figure 5. Top panel: Σ_{CO} BIMA data ($\theta_{FWHM} = 10.43 \times 9.19$ arcsec^2). Contour levels are (5, 10, 15, 20, 30, 40, 50, 60) Jy beam^{-1} km s^{-1}. Bottom panel: the intensity-weighted mean velocity field of NGC 470. Contour levels are (2260, 2280, 2300, . . . , 2440) km s^{-1}.

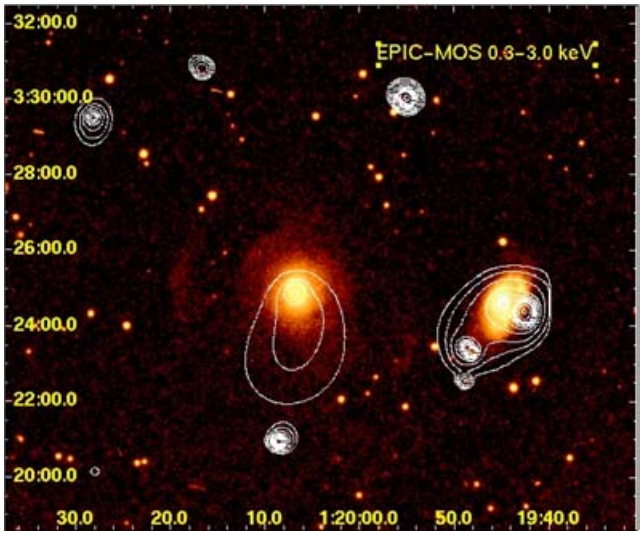

Figure 6. X-ray isointensity contours of the emission in the 0.3–3 keV band.

To convert the count rates into fluxes and luminosities, we have assumed a conversion factor based on the EPIC–PN camera, since neither source is affected by the CCD gaps. The conversion factor is derived from XSPEC assuming a power-law model with $\Gamma = 1.7$ and line-of-sight galactic N_H. The assumption of a thermal plasma spectrum would hardly change the resulting fluxes.

4 DISCUSSION

Cosmological simulations show that hierarchical galaxy formation is an ongoing process even at the present epoch (see e.g. Murali et al. 2002), a result consistent with the presence of systems in the local universe that shows signatures of major and minor mergers (see e.g. Struck 1999). Nearby interacting galaxies, then, allow us to study the galaxy evolution caused by encounters (even unbound), accretion events, minor and major mergers. Arp 227 is a prototypical example of an encounter in a low-density environment.

4.1 Comparison between the gas and the stellar kinematics

A first indication of the degree of the interaction and of possible hints relevant to its history comes from the comparison between the stellar and gas velocity fields since the stellar velocity field should trace the galaxy potential.

Models of galaxy–galaxy interactions show that the gaseous component is gravitationally perturbed in two slightly different ways. The first is the direct tidal force, which is exerted on both the stars and the gas. The second is the reaction of the gas to tidal deformation of the galaxy potential. In addition, there may be direct gas-dynamical interaction in the form of ram-pressure if both members of the pair contain gas (not the case for Arp 227). Galaxies sometimes contain stellar or gas components with misaligned or even opposite angular momenta. This phenomenon, which is typically attributed to the accretion of gas or stars from a companion or minor merger, is found not only in early-type galaxies, but also in spirals (see e.g. Corsini & Bertola 1998; Bertola et al. 1999; Sarzi et al. 2000; Corsini, Pizzella & Bertola 2002).

The velocity profiles of the warm gas and stars of NGC 470 have been obtained along PA = 155° by Vega Beltran et al. (2001) and Héraudeau et al. (1999). Fig. 7 shows the comparison with our data, obtained from our velocity field simulating a long-slit observation with the same position angle. We have already discussed above the presence of the secondary components in the Hα line. In obtaining the velocity profile along PA = 155°, which directly crosses the area in which secondary components are present, we used, for the comparison, the main component as representative of the gas motion in the bulge and the disc of NGC 470. The above authors did not mention the presence of secondary components that can be separated and analysed in our 2D data.

Fig. 7 shows the agreement between the stellar and the gas kinematics; gas and stars have similar and very low velocity dispersion [(see table 1 from Vega Beltran et al. (2001))]. Note however that stars have a velocity gradient shallower than gas in the central part.

For the ionized gas, the comparison shows a general agreement, within the errors, between our and literature data in the galaxy outskirts. In the central ±10 arcsec, the Vega Beltran et al. (2001) velocity profile, obtained from the [O III](λ5007Å) line, is systematically steeper than that of ours. This effect can probably be explained (at least partly) by better seeing conditions (1.2 arcsec versus our 3 arcsec).

Fig. 8 shows the superposition of our Hα, H I and CO($J = 1 - 0$) rotation curves, obtained adopting an inclination $i = 55°$ and an heliocentric velocity $V_{hel} = 2384$ km s^{-1}. CO and Hα rotation

Table 3. Summary of results.

	NGC 470	NGC 474
X-ray data		
PN counts	175±23	75.2±15
Count rate (counts s^{-1})	3×10^{-2} $\pm4\times10^{-3}$	1.2×10^{-2} $\pm2.3\times10^{-3}$
Flux (0.5–2 keV)[erg s^{-1} cm^{-2}]	5.1×10^{-14}	1.0×10^{-14}
log L_X (0.5–2 keV) [erg s^{-1}]	39.79	39.05
log L_B [$L_\odot$] [erg s^{-1}]	10.18	10.24
log L_X/L_B [erg s^{-1} $L^{-1}_\odot$] (0.5–2 keV)	29.61	28.81
Hα data		
Inclination adopted (°)	55	
V_{hel} adopted [km s^{-1}]	2384	
Max. rotation V_{max} [km s^{-1}]	≈240	
H I data		
Max. rotation V_{max} [km s^{-1}]	≈240	
MH I [$M_\odot$]	4.3×10^9	
MH I/L_B [$M_\odot/L_\odot$]	0.28	
R_{HI} [arcmin], [kpc] tail	≈8.5, 78.4	
Fract. of H I mass in tail	10 per cent	
CO data		
M(H_2) [$M_\odot$]	1.6×10^9	
M(H_2)/L_B [$M_\odot/L_\odot$]	0.11	
R_{CO} [arcsec], [kpc]	≈27, 4.1	

curves are comparable within errors in the inner parts (30 arcsec). The low resolution of the H I data prevents such a comparison in the inner 80 arcsec while the Hα and H I curves are consistent at ≈100 arcsec. The comparison of the warm and the cold gas rotation curves supports the idea that the inner parts of NGC 470 [up to ≈2.8 $A_e(B)$] are unaffected by the ongoing interaction, which is clearly detectable well outside the optical galaxy in the H I tidal extension and in the indication of a warp in the H I disc.

4.2 The Hα secondary components in NGC 470: gas inflow or an old accretion?

First, we note that from the dynamical information alone we cannot distinguish between radial inflow or radial outflow. The two Hα components that do not follow the rotation of the NGC 470 disc are therefore equally consistent with inflow or outflow. Hα outflows are often seen in starburst objects (e.g. M82) and NGC 470 is undergoing an intense burst of star formation (Devereux 1989) and it does have a centrally concentrated Hα distribution. However, the S-shaped distribution of the secondary components (Figs 2c and d) is not seen in the total Hα emission (Fig. 2a). It is difficult to reconcile this with an outflow of gas that would occur perpendicular to the disc. The morphology of the secondary Hα components is evidence of a radial component of motion in the plane of the disc, and we consider only the inflow hypothesis in what follows.

It is widely believed that perturbation of the stellar $m = 2$ mode is the key mechanism in initiating radial gas inflow. The bar created in the stellar disc as a direct consequence of the tidal force

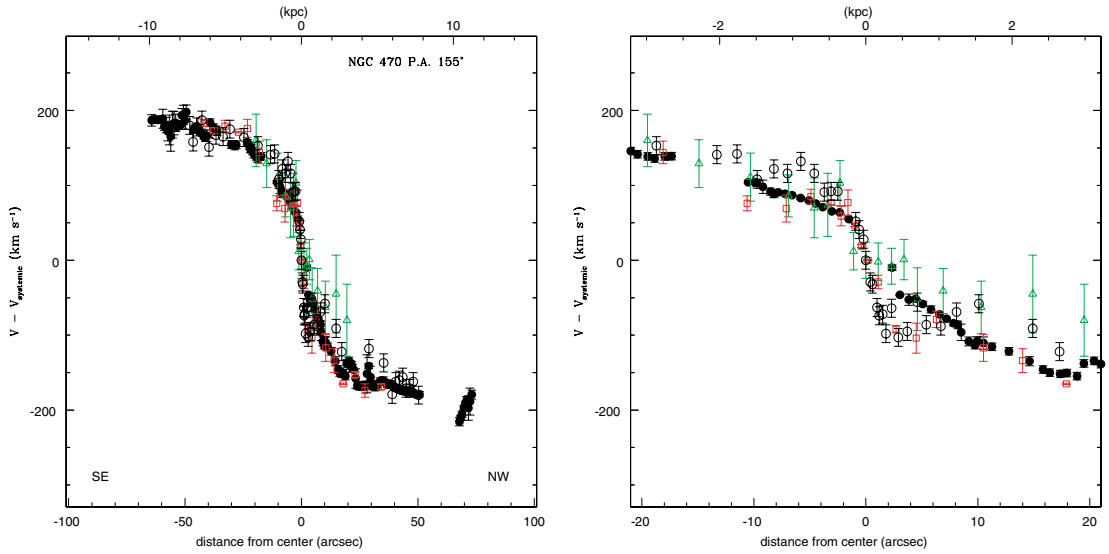

Figure 7. Left-hand panel: comparison between our Hα velocity profile (full circles) along PA = 155° and observations obtained by Vega Beltran et al. (2001) [the gas component (O III line: open circles), stars (open squares)] and Héraudeau et al. (1999) (stars: open triangles). Right-hand panel: enlargement of the central 20 arcsec.

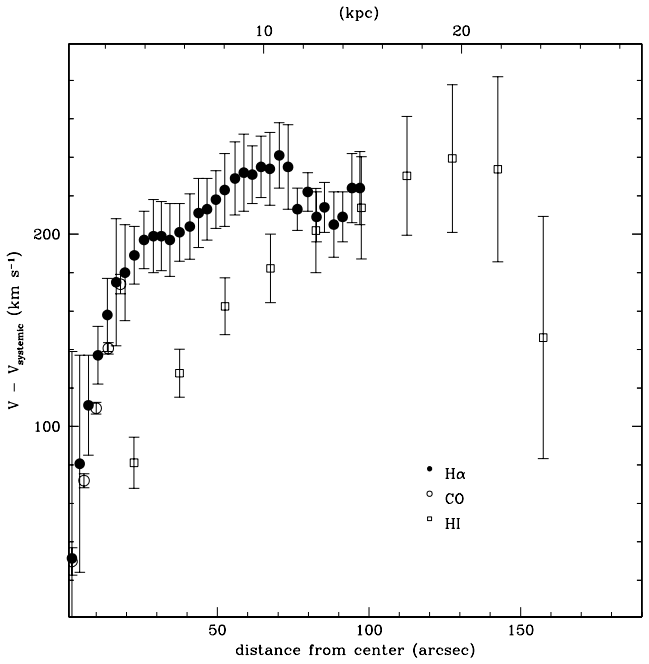

Figure 8. Composite rotation curve of NGC 470. The rotation curve is obtained adopting a PA $= -32^{\circ}$ and an inclination of 55°.

exerted by a perturber has gained ground as one of the mechanisms able to induce gas flows towards the galaxy centre from the onset of the encounter (see e.g. Noguchi 1988; Gerin, Combes & Athanassoula 1990; Salo 1991; Miwa & Noguchi 1998; Berentzen et al. 2004). Several observations have shown that gas flows inwards (see e.g. Downes et al. 1996; Regan, Sheth & Vogel 1999; Sheth et al. 2000, 2002) and accumulates in the centre (see e.g. Sakamoto et al. 1999b; Sheth et al. 2005).

Cross-fuelling via small accretions from interacting companions may also be a source of gas infall to the galaxy centre (see e.g. Salo & Laurikainen 1993). Small accretions should mark the history of galaxies not only modifying their photometric properties, but possibly also inducing star formation episodes. Observed kinematical phenomena retain a memory of accretion processes (the misalignment of stellar and gas components mentioned above is an example of this).

The merging with a faint companion seems to be the driver of the secular evolution of the S0 NGC 474, as suggested by the shell system and the peculiar stellar kinematics in the central regions (see e.g. Hau et al. 1996; Pierfederici & Rampazzo 2004). It is more difficult to suggest an accretion/minor merger as responsible for the secondary Hα components in the centre of the gas-rich spiral NGC 470.

This study shows that NGC 474 is a very 'gas-poor' S0. This seems to exclude a cross-fuelling/accretion from this galaxy to NGC 470. Furthermore, the agreement between the stellar and Hα velocity profile (see Fig. 7) suggests that the material traced by the second component in the Hα line profile does not have a large velocity shift with respect to the stars. This may argue against an accretion origin unless the accretion event occurred sufficiently long ago that the accreted gas now follows the disc gas as a result of cloud–cloud collisions.

There is another argument that supports the idea that the secondary components have not been accreted but have an internal origin. Recently, Iono, Yun & Mihos (2004) studied the detailed gas response during disc–disc (gas-rich) galaxy collisions. Models suggest that in the first phases of an encounter, the distribution of gas shows a significant evolution and can supply a substantial amount of gas to the nuclear region giving rise to the presence of non-circular motions. We commented above on the geometrical decoupling between the bar and the filamentary structure of the area in which the double components in the Hα line is found. Iono et al. (2004) simulations show that the stars respond to the tidal interaction by forming both transient arms and long-lived $m = 2$ bars, but the gas response is more transient, flowing directly towards the central regions within 10^8 yr after the initial collision.

Furthermore, Iono et al. (2004) try to characterize the fraction of molecular gas to the total gas mass in order to determine a 'merger chronology'. They compute the variation of the molecular gas mass fraction ($M_{\rm H_2}/M_{\rm H\,I+H_2}$) during the simulated collisions assuming an initial value of ($M_{\rm H_2}/M_{\rm H\,I+H_2}$) of 0.25, consistent with the mean empirical ratio derived by Casoli et al. (1998) on a sample of 582 galaxies. The sharp rise in the molecular fraction occurs $\approx 1.0 \times 10^8$ yr after the pericentric passage rising up to a value of 0.6. Our measured value of ($M_{\rm H_2}/M_{\rm H\,I+H_2}$) is 0.27 indicating that the encounter is in a very early stage since the above value is indistinguishable from that derived from a non-interacting sample.

4.3 Mass distribution in NGC 470 from the composite rotation curve

Although NGC 470 is interacting with the companion NGC 474, our data show that there are modest perturbations in the inner kinematics of the galaxy. Using the surface photometry of NGC 470 obtained by Pierfederici & Rampazzo (2004), we attempt to model the mass distribution of the galaxy using a composite rotation curve obtained from Hα and H I rotation curves. The method we used is described in Carignan (1985) and Blais-Ouellette et al. (1999). The luminosity profile is transformed into a mass distribution assuming radially constant mass-to-light ratio (M/L). There are therefore three free parameters: the M/L for the luminous matter (disc+bulge) and ρ_0, the central density and r_0, the core radius for the dark halo modelled as an isothermal sphere. A best-fitting routine minimizes χ^2 in the 3D parameter space.

Fig. 9 shows an attempt to model the rotation curve of NGC 470. In this case, the best fit of the rotation curve is obtained assuming a dark halo with a very low central density and a large core radius. At about 50 arcsec from the centre, the model reaches the plateau ($\sim$220 km s^{-1} at about 8 kpc). This fit gives a reasonable M/L $=$ 2.0 $\mathrm{M_\odot\,L_\odot^{-1}}$ for the bulge and M/L $= 5.0\ \mathrm{M_\odot\,L_\odot^{-1}}$ for the disc (see e.g. Garrido 2003). A Navarro, Frenk & White (1996) profile could give a good fit to the kinematic data but does not reproduce the luminosity profile where a bulge component is present in the data.

4.4 The X-ray luminosity of Arp 227

The diffuse X-ray emission from the hot intra-group medium (IGM), detected not only in compact but also in loose groups, is often taken as the direct evidence of the group potential (Mulchaey et al. 1993; Pildis 1995; Mulchaey et al. 1996; Ponman et al. 1996; Mulchaey & Zabludoff 1998). The first studies that tried to classify poor groups into an evolutionary sequence, combining their X-ray properties with galaxy population (presence of satellite galaxies, ratio between early- and late-type galaxies, etc.) and group dynamical information, suggest that groups could fall into different classes defined by their X-ray properties (Zabludoff 1999). Groups with extended, hot IGM

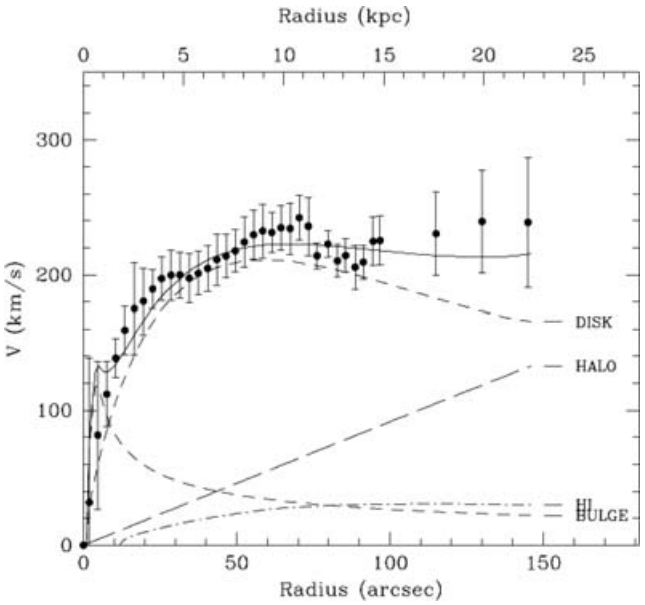

Figure 9. Mass model for NGC 470 (see text). The sum of the components (continuous line) and the contributions of each component (short dashed – disc & bulge; long dashed – dark halo component; dots & dashed – H I disc) are shown. We assume a spherical and symmetric dark matter distribution following an isothermal sphere profile $\rho(r) = \rho_0/1+(r/R_0)^2$.

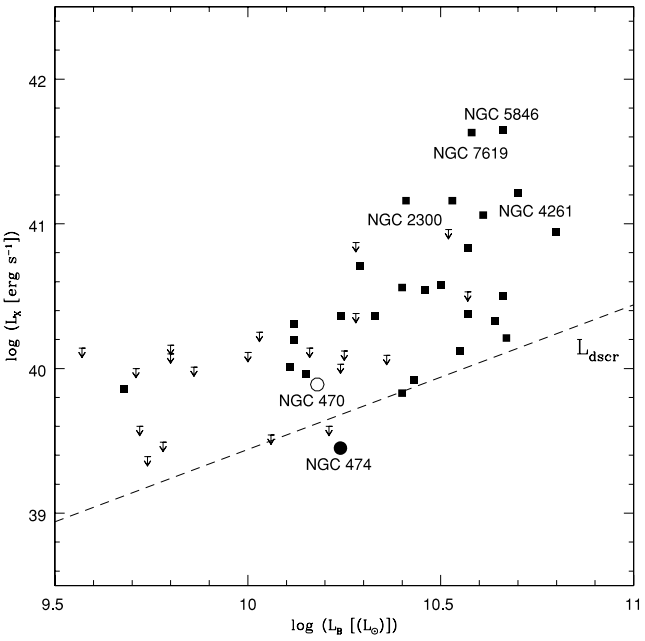

Figure 10. NGC 470 and 474 in the $L_B - L_X$ plane. For comparison, we plot also early-type galaxies with fine structure, indicative of *dynamically young* galaxies, from the sample of Sansom et al. (2000) from which we removed three objects (namely NGC 3605, 3998 and 4203) having LINER/AGN activity (see text). X-ray luminosities are taken from the O'Sullivan et al. (2001) compilation. We have re-calculated the luminosity, given in Table 3, adopting their recipe. We have labelled galaxies in this sample that are members of poor groups (see e.g. Helsdon et al. 2001). The dashed line (L_{dscr}) represents the expected contribution from discrete stellar X-ray sources from Ciotti et al. (1991). Filled squares are detections, and arrows denote upper limits.

also have a giant elliptical, typically the brightest group galaxy, lying near or at the peak of the 'smooth, symmetric' X-ray emission. Mulchaey & Zabludoff (1998) suggest that this could represent a low-mass version of clusters. In contrast, there are groups without diffuse X-ray emission composed of bright late-type galaxies and their satellites. If the group evolution is such that systems dominated by late-type objects could evolve into groups dominated by a central, giant elliptical and a detectable IGM, then we expect to find *transition systems*. These 'evolving groups' have signatures of the recent dynamical evolution in their cores, including interacting galaxies, and any extended X-ray emission is not regular and peaked on a single central galaxy.

The study of the X-ray emission has also been extended to samples of physical pairs (Rampazzo et al. 1998; Henriksen & Cousineau 1999; Trinchieri & Rampazzo 2001) in an attempt to connect the pair to group X-ray properties. They found that the distribution of L_X and L_X/L_B encompasses the whole range of early-type galaxies, in spite of the very small number of objects studied. Furthermore, a group-like extension of the diffuse X-ray emission has been detected in some pairs.

In Fig. 10, we show the location of NGC 474 and 470 in the log L_B–log L_X plane. In the same figure we plot, for comparison, the sample of early-type galaxies with Σ, the fine structure parameter, taken from Sansom, Hibbard & Schweizer (2000). From the sample, we removed three objects having LINER/AGN activity, namely NGC 3605 (see e.g. Eracleous & Halpern 2001), NGC 3998 (see e.g. Ho et al. 1997, and reference therein) and NGC 4203 (see e.g. Ho & Ulvestad 2001, and reference therein).

The Σ parameter is an empirical measure of the optical disturbance present in a galaxy since its value is given by a combination of the optical strength of ripples, the number of detected ripples, the number of jets, an estimate of boxiness and the presence of X-structures. The higher the value of Σ the higher the morphological disturbance and the probability that the galaxy is *dynamically young*. The high Σ value of 5.26 for NGC 474 (Sansom et al. 2000), together with the decoupled stellar core (Hau et al. 1996), is then both indicative of a dynamically young object.

Sansom et al. (2000) sample includes galaxies which are the dominant members of poor groups (see e.g. Mulchaey et al. 1993; Helsdon et al. 2001) which we indicate in Fig. 10. According to Helsdon et al. (2001), the X-ray emission from these early-type galaxies may be the focus of group cooling flows. Note that the X-ray emission is often associated with groups containing very few galaxies, *overlapping the domain of classical pairs*. NGC 2300, shown in the figure, is the best-known example of this overlap (Mulchaey et al. 1993). This group is dominated by a bright mixed morphology pair of galaxies (NGC 2276 and 2300) that is isolated enough to satisfy the isolation criterion used for the Catalogue of Isolated Pairs (Karachentsev 1987; KPG 127). However, two significantly fainter galaxies (NGC 2268 and IC455; ∼2-mag fainter), at the save velocity of the pair, are thought to belong to the loose group centred on NGC 2300 (Mulchaey et al. 1993).

Tully (1988) included both NGC 470 and 474 within a very loose sub-structure ($52 - 12 + 12$) of the Cetus–Aries cloud together with another four widely separated galaxies (namely NGC 488, 493, 520 and UGC 871). Following recent redshift measures, all members of this sub-structure lie within a velocity range of 213 km s^{-1}.

Our study shows that NGC 474 belongs both to the class of interacting pairs, as indicated by the H I tail of its companion NGC 470, and to poor groups. Our H I observations detect two faint, gas-rich companions, MCG 00-04-083, ∼10 arcmin south of NGC 470 and the galaxy called [HDL96] 385-007 in NED ∼ 20 arcmin to the

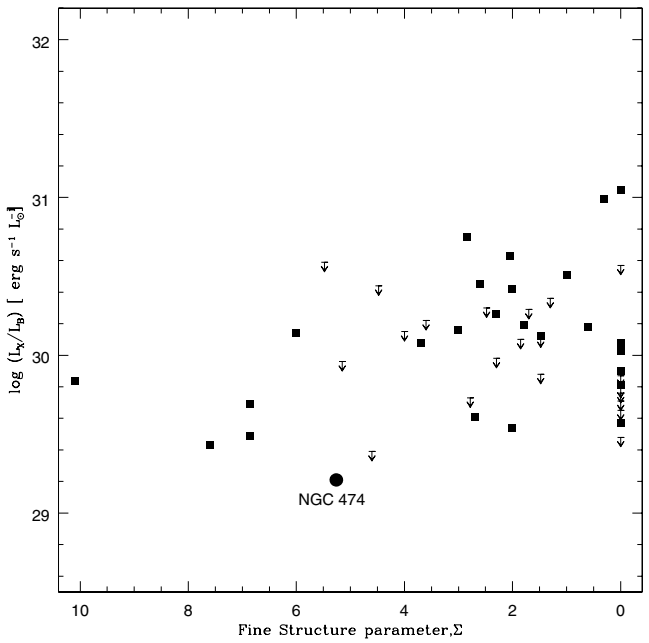

Figure 11. Position of NGC 474 in the normalized X-ray luminosity versus fine structure parameter Σ for early-type galaxies. Symbols are the same as in Fig. 10.

south. Furthermore, Pierfederici & Rampazzo (2004) suggest that the properties of the NGC 474 system of shells provide evidence of a recent merging episode with a former companion. However, its X-ray characteristics are not in line with other dominant members of groups. As shown by Fig. 10, the X-ray luminosity emission of NGC 474 lies about two orders of magnitude below that of dominant group members and is located in the area of the log L_B–log L_X plane where the X-ray emission could be explained by the superposition of discrete X-ray sources. Recent *XMM–Newton* and *Chandra* observations by O'Sullivan & Ponman (2004) detected three underluminous elliptical galaxies (NGC 3585, 4494 and 5322), all of which show evidence of recent dynamical disturbances, including kinematically distinct cores as in the case of NGC 474. These are also in the region consistent with emission from discrete sources only, although not as extreme as NGC 474.

In Fig. 11, we reproduce the plot of Sansom et al. (2000) using the revised X-ray luminosities from O'Sullivan, Forbes & Ponman (2001). Sansom et al. (2000) and O'Sullivan et al. (2001) interpret the negative trend observed between L_X/L_B (linked to the gas content in early-type galaxies) and Σ (linked to the age/dynamical stage) as evidence that several gigayears are required for the build-up of hot gaseous haloes, so that recent mergers/young systems are deficient in hot gas. O'Sullivan et al. (2001) also attribute some of the scatter seen in the global L_X versus L_B relation to the evolutionary stage and past merger history of early-type galaxies. NGC 474 is at the bottom of both distributions. This gives support to the idea that NGC 474 is a young galaxy that has recently undergone a (minor) merging episode (as also suggested by the presence and characteristics of the shell system). As a result, the system has not had time to build-up a massive, relaxed hot halo around the galaxy that could be detected in X-rays. The lack of group-type extended emission is also not peculiar to NGC 474. Several other young systems, though in small groups, do not show extended emission at very low levels: all the three X-ray faint galaxies in O'Sullivan et al. (2001) lack a substantial group component. This might also indicate an early stage for the group around these systems, or simply a poorer/cooler environment that has escaped detection.

5 SUMMARY AND CONCLUSIONS

We have investigated the hot, warm and cold gas properties in Arp 227 using *XMM–Newton*, GHASP Fabry–Perot instrument, archival H I VLA observations and BIMA CO ($J = 1 - 0$) observations.

We attempt to infer the evolutionary phase of this interacting pair composed of a spiral, NGC 470, and a lenticular, NGC 474, galaxy.

(i) The most evident signature of interaction lies in the H I distribution which shows a gas tail connecting the spiral member, NGC 470, to the lenticular, NGC 474. The H I disc appears warped.

(ii) Our measure of the value of $(M_{H_2}/M_{H I+H_2})$ is 0.27 suggesting that the encounter is in a very early stage according to models of gas evolution during galaxy–galaxy encounters (see Iono et al. 2004). During the first phase of an encounter, these models predict a strong gas infall towards the galaxy centre.

(iii) Secondary components in the Hα emission appear at the centre of NGC 470, separated from the main one which maps a nearly unperturbed velocity field. The filamentary shape and the velocities of these patches of ionized gas superimposed on to the central parts of the disc of NGC 470 suggest that these clouds mark a probable gas infall.

(iv) The main, nearly unperturbed trend of the kinematics is confirmed by CO observations, although restricted to the centre of NGC 470.

(v) The NGC 470 mass model shows that in the inner 20 kpc the disc component is dominant.

(vi) The X-ray luminosity of NGC 470 is comparable with that of a 'normal' spiral galaxy. The gas content of NGC 474 is very low, if any. The galaxy has not been detected in Hα and its X-ray luminosity is consistent with emission from discrete sources. The X-ray luminosity of NGC 474 is, in particular, about 2 orders of magnitude lower than that of early-type galaxies at the centre of X-ray luminous poor groups. There is no evidence of emission from a group potential. This could be an additional evidence that the pair is at an early stage of its evolution and the build-up of the IGM has just begun.

Both the large NGC 474 shell system, probably produced by a merging episode, and the gas-rich, faint late-type companions detected in H I south of NGC 470 suggest that Arp 227 could be a possible poor group and could then represent the evolution in low-density environments. Indeed, both the $(M_{H_2}/M_{H I+H_2})$ and L_X/L_B ratios for NGC 470 are indistinguishable from those of isolated galaxies. If it is a bound system, Arp 227 is a snapshot of a group in the early phases of its evolution whose drivers are the accretion of faint companions and the ongoing large-scale interaction between the dominant members NGC 470 and 474.

ACKNOWLEDGMENTS

CC acknowledges support from the Conseil de Recherches en Sciences Naturelles et en Genie du Canada and from the Fonds Quebecois de Recherche sur la Nature et les Technologies. KS acknowledges funding from the Owens Valley Millimeter Array and California Institute of Technology which are partially supported by NSF grant AST-9981546 and the Norris Foundation. The BIMA Array is operated with support from NSF grant AST-9981289. This research has made use of the NASA/IPAC Extragalactic Database (NED) which is operated

by the Jet Propulsion Laboratory, California Institute of Technology, under contract with the National Aeronautics and Space Administration. The DSS was produced at the Space Telescope Science Institute under U.S. Government grant NAG W-2166. The images of these surveys are based on photographic data obtained using the Oschin Schmidt Telescope on Palomar Mountain and the UK Schmidt Telescope. The plates were processed into the present compressed digital form with the permission of these institutions.

REFERENCES

Amram P., Balkowski C., Boulesteix J., Cayatte V., Marcelin M., Sullivan W., 1996, A&A, 310, 737
Balcells M., Quinn P., 1990, ApJ, 361, 381
Barnes J., 1996, Galaxies: Interactions an Induced Star Formation (26th Saas-Fee Advanced Course). Springer, New York, p. 275
Berentzen I., Athanassoula E., Heller C. H., Fricke K. J., 2004, MNRAS, 347, 220
Bertola F., Corsini E. M., Vega-Beltrán J., Pizzello A., Sarzi M., Cappellari M., Funes J. G., 1999, ApJ, 519, L17
Blais-Ouelette S., Carignan C., Amram P., Côtè S., 1999, AJ, 118, 2123
Boulesteix J., 1999, User Manual of ADHOCw Reduction Package. Observatoire de Marseille, Marseille
Bower R. G., Balogh M. L., 2004, in Mulchaey J. S., Dressler A. D., Oemler A., eds, Carnegie Observatories Astrophysics Ser. Vol. 3, Clusters of Galaxies: Probes of Cosmological Structure and Galaxy Evolution. Cambridge University Press, Cambridge, p. 326
Carignan C., 1985, ApJ, 299, 59
Casoli F. et al., 1998, A&A, 331, 451
Ciotti L., Pellegrini S., Renzini A., D'Ercole A., 1991, ApJ, 376, 380
Corsini E. M., Bertola F., 1998, J. Korean Physical Soc., 33, 574
Corsini E. M., Pizzella A., Bertola F., 2002, A&A, 382, 48
de Vaucouleurs G., de Vaucouleurs A., Corwin H. G., Jr, Buta R. J., Paturel G., Fouque P., 1991, Third Reference Catalogue of Bright Galaxies. Springer, New York
Devereux N. A., 1989, ApJ, 346, 126
Diaferio A., Geller M. J., Ramella M., 1994, AJ, 107, 868
Domingue D. L., Sulentic J. W., Xu C., Mazzarella J., Gao Y., Rampazzo R., 2003, AJ, 125, 555
Downes D., Reynaud D., Solomon P. M., Radford S. J. E., 1996, ApJ, 461, 186
Dupraz C., Combes F., 1986, A&AS, 166, 53
Eracleous M., Halpern J. P., 2001, ApJ, 554, 240
Friedli D., Wozniak H., Rieke M., Bratschi P., Mertinet L., 1996, A&AS, 118, 461
Gach J.-L. et al., 2002, PASP, 114, 1043
Garrido O., 2003, PhD thesis, Université de Provence
Gerin M., Combes F., Athanassoula E., 1990, A&A, 230, 37
Governato F., Tozzi P., Cavaliere A., 1996, ApJ, 458, 18
Hau G. K. T., Thomson R. C., 1994, MNRAS, 270, L23
Hau G. K. T., Balcells M., Carter D., 1996, in Bender R., Davies R., ed., Proc. IAU Symp. 171, New Light on Galaxy Evolution. Kluwer, Dordrecht, p. 338
Helsdon S. F., Ponman T. J., O'Sullivan E., Forbes D. A., 2001, MNRAS, 325, 693
Henriksen M., Cousineau S., 1999, ApJ, 511, 595
Héraudeau P., Simien F., Maubon G., Prugniel P., 1999, A&A, 136, 509
Hernandez-Toledo H. M., Puerari I., 1999, AJ, 118, 108
Hernandez-Toledo H. M., Dultzin-Hacyan D., Sulentic J. W., 2001, AJ, 121, 1319
Hernquist L., Quinn P., 1987a, ApJ, 312, 1
Henquist L., Quinn P., 1987b, ApJ, 312, 17
Hernquist L., Spergel D. N., 1992, ApJ, 399, L117
Ho L. C., Filippenko A. V., Sargent W. L. W., Peng C. Y., 1997, ApJS, 112, 391
Ho L. C., Ulvestad J. S., 2001, ApJS, 133, 77
Iono D., Yun M. S., Mihos C. J., 2004, ApJ, 616, 199
Iono D., Yun M. S., Ho P. T. P., 2005, ApJS, 158, 1
Karachentsev I. D., 1987, Dvoinye Galaktiki. Nauka, Moskow
Kormendy J., 1984, ApJ, 287, 577
Laval A., Boulesteix J., Georgelin Y. P., Georgelin Y. M., Marcelin M., 1987, A&A, 175, 199
Lewis I. et al., 2002, MNRAS, 334, 673
Longhetti M., Bressan A., Chiosi C., Rampazzo R., 1999, A&A, 345, 419
Longhetti M., Bressan A., Chiosi C., Rampazzo R., 2000, A&A, 353, 917
Malin D., Carter D. F., 1983, ApJ, 274, 534
Miwa T., Noguchi M., 1998, ApJ, 499, 149
Mulchaey J. S., Davis D. S., Mushotzky R. F., Burstein D., 1993, ApJ, 404, L9
Mulchaey J. S., Davis D. S., Mushotzky R. F., Burstein D., 1996, ApJ, 456, 80
Mulchaey J. S., Zabludoff A., 1998, ApJ, 496, 73
Mulchaey J. S., 2000, ARA&A, 38, 289
Murali C., Katz N., Hernquist L., Weinberg D. H., Davé R., 2002, ApJ, 571, 1
Navarro J. F., Frenk C. S., White S. D. M., 1996, ApJ, 462, 563
Nikolic B., Cullen H., Alexander P., 2004, MNRAS, 355, 874
Noguchi M., 1987, MNRAS, 228, 635
Noguchi M., 1988, A&A, 203, 259
O'Sullivan E., Forbes D. A., Ponman T. J., 2001, MNRAS, 328, 461
O'Sullivan E., Ponman T. J., 2004, MNRAS, 349, 535
Pierfederici F., Rampazzo R., 2004, AN, 325, 359
Pildis R., 1995, ApJ, 443, 514
Ponman T. J., Bourner P. D. J., Ebeling H., Bohringer H., 1996, MNRAS, 283, 690
Ramella M., Diaferio A., Geller M. J., Huchra J. P., 1994, AJ, 107, 1623
Rampazzo R., Sulentic J. W., 1992, A&A, 259, 43
Rampazzo R., Covino S., Trinchieri G., Reduzzi L., 1998, A&A, 330, 423
Ravindranath S., Ho L., Peng C. Y., Filippenko A. V., Sargent W. L., 2001, AJ, 122, 653
Regan M. W., Sheth K., Vogel S. N., 1999, ApJ, 526, 97
Sakamoto K., Okumura S. K., Ishizuki S., Scoville N. Z., 1999b, ApJ, 525, 691
Salo H., 1991, A&A, 243, 118
Salo H., Laurikainen E., 1993, ApJ, 410, 586.
Sansom A. E., Hibbard J. E., Schweizer F., 2000, AJ, 120, 1946
Sarzi M., Corsini E. M., Pizzella A., Vega Beltrán J. C., Cappellari M., Funes J. G., Bertola F., 2000, A&A, 360, 439
Sault R. J., Teuben P. J., Wright M. C. H., 1995, in Shaw R. A., Payne H. E., Hayes J. J. E., eds, ASP Conf. Ser. Vol. 77, Astronomical Data Analysis Software and Systems IV. Astron. Soc. Pac., San Francisco, p. 433
Schiminovich D., Van Gorkom J. H., Van der Hulst T., Oosterloo T., Wilkinson A., 1997, in Arnaboldi M., Da Costa G. S., Saha P., eds, ASP Conf. Ser. Vol. 116, The Second Stromlo Symposium: The Nature of Elliptical Galaxies. Astron. Soc. Pac., San Francisco, p. 362
Shombert J. M., Wallin J. F., 1987, AJ, 94, 300
Schweitzer F., Seitzer P., Faber S. M., Burstein D., Dalle Ore C. M., Gonzalez J. J., 1990, ApJ, 364, L33
Sheth K., Regan M. W., Vogel S. N., Teuben P. J., 2000, ApJ, 532, 221
Sheth K., Vogel S. N., Regan M. W., Teuben P. J., Harris A. I., Thornley M. D., 2002, AJ, 124, 2581
Sheth K., Vogel S. N., Regan M. W., Thornley M. D., Teuben P. J. 2005, ApJ, 632, 217
Simien F., Prugniel Ph., 2000, A&AS, 145, 263
Struck C., 1999, Phys. Rep., 321, 1
Sulentic J. W., 1989, AJ, 98, 2066
Thomson R. C., 1991, MNRAS, 253, 256
Trinchieri G., Rampazzo R., 2001, A&A, 374, 454
Tully B. R., 1988, Nearby Galaxies Catalog. Cambridge Univ. Press, Cambridge
Turnbull A. J., Bridges T. J., Carter D., 1999, MNRAS, 307, 967
Vega Beltran J. C., Pizzella A., Corsini E. M., Funes J. G., Zeilinger W. W., Beckman J. E., Bertola E., 2001, A&A, 374, 394

Verdes-Montenegro L., Yun M. S., Perea J., del Olmo A., Ho P. T. P., 1998, ApJ, 497, 89
Xu C., Sulentic J. W., 1991, ApJ, 374, 407
Xu C., Gao Y., Mazzarella J., Lu N., Sulentic J. W., Domingue D. L., 2000, ApJ, 541, 644
Zabludoff A., 1999, in Whitelock P., Cannon R., eds, IAU Symp. 192, The Stellar Content of the Local Group. Astron. Soc. Pac., San Francisco, p. 433
Zepf S. E., 1993, ApJ, 407, 448
Zepf S. E., Whitmore B. C., 1991, ApJ, 383, 542

APPENDIX A: THE X-RAY SOURCE WEST OF NGC 470

We have investigated the spectral properties of the source West of NGC 470 to determine its nature and its possible association with the galaxy.

Counts are derived in a circle of radius 30 arcsec above a background chosen in an area between NGC 470 and 474. The resulting net counts in the 0.3–5.0 keV band are 640±26 and do not allow us to unambiguously determine which spectral model best characterizes the data; however, in the assumption of simple models, such as bremsstrahlung or power law, the best fits indicate a hard spectrum (kT∼8 keV or $\Gamma = 1.6$) with higher than galactic line-of-sight absorbing columns ($\sim 1 - 1.4 \times 10^{21}$ cm^{-2}). The luminosity associated with this source, if at the distance of NGC 470, is $L_X(0, 5\text{–}2\,\mathrm{keV}) \sim 6 \times 10^{40}$ erg s^{-1} and $L_X(2\text{–}10\,\mathrm{keV}) \sim 4 \times 10^{40}$ erg s^{-1}, respectively. The spectral properties and the high luminosity argue against a source in the galaxy and suggest that the source is a background object. The high absorbing column could just indicate that the source is behind the H I envelope but still within the galaxy. However the high luminosity, in particular considering both the off-nuclear position and the luminosity coming from the inner regions of the galaxy, argues against it being a source of NGC 470. The search for the optical counterpart might be very difficult, however, given the brightness of the galaxy.

This paper has been typeset from a TEX/LATEX file prepared by the author.